Cell, Volume *139*

Supplemental Data

Condensins Regulate Meiotic DNA Break Distribution, thus Crossover Frequency, by Controlling Chromosome Structure

David G. Mets and Barbara J. Meyer

SUPPLEMENTAL EXPERIMENTAL PROCEDURES

Immuno-precipitation Analysis

To prepare whole worm extracts, animals were grown either as a mixed stage population, or to the L4 stage as a synchronized population on 10 cm NG agar plates with an OP50 lawn. At the proper stage animals were washed 3 times in M9 buffer and twice in homogenization buffer (50 mM HEPES-KOH [pH 7.6], 1 mM EDTA, 140 mM KCl, 0.5% NP-40, 10% glycerol). The worm/homogenization buffer mixture was frozen in liquid nitrogen and macerated with a mortar and pestle cooled to liquid nitrogen temperature. Frozen powder was placed in 1.5 ml eppendorf tubes and stored at -80˚C. 1 ml macerate aliquots were thawed on ice and centrifuged at 4˚C for 1 min at 16,000 x g. The supernatant was passed over a 1 ml bed volume Sephadex s-100 (Sigma-Aldrich) column pre-equilibrated with IP buffer (50mM HEPES-KOH [pH 7.6], 1mM EDTA, 250 mM KCL, 0.05% NP-40) at 4˚C. The second and third 1 ml column fractions were pooled and frozen in liquid nitrogen in 100 µl aliquots.

For each immuno-precipitation, one 100 µl aliquot was thawed on ice, added to 900 µl of IP buffer, and passed through a 27.5 gauge hypodermic needle 6 times. Following addition of 10 - 40 µg of antibodies, this mixture was nutated at 4˚C for 4 hr, after which 15 µl of protein-A conjugated sepharose beads (Invitrogen) were added. Following 30 min of nutation at 4˚C, the samples were centrifuged at 4˚C for 2 min at 400 x g, and the supernatant was discarded. The beads were then washed 4 times in 1 ml of IP buffer with a 2 min, 400 x g centrifugation between each wash. Antibody-protein complexes were eluted by boiling in SDS sample buffer, subjected to SDS-PAGE on a 3-8% 1 mm Novex gel (Invitrogen), and transferred to nitrocellulose membrane. For immuno-detection, the membrane was incubated in primary antibody and detected with the appropriate secondary antibody-HRP (Roche) conjugate and ECL plus (GE). For mass-spectrometry, ten individual DPY-26 IPs were combined into a single lane, and, after SDS-PAGE, visualized with colloidal coomassie blue staining. MALDI-TOF mass spectrometry of trypsinized bands cut from the SDS-PAGE gel identified DPY-26, DPY-27, DPY-28, MIX-1, and SMC-4 (Supplemental Table 1).

Antibodies

Antibodies against DPY-26 (Lieb et al., 1996), DPY-28 (Tsai et al., 2008), DPY-27 (Chuang et al., 1994), SMC-4 (Hagstrom et al., 2002), HCP-6 (Chan et al., 2004), MIX-1 (Hagstrom et al., 2002), SMC-3 (Chan et al., 2003), RAD-51 (Alpi et al., 2003), and HTP-3 (Bhalla and Dernburg, 2005) have all been described previously. The anti-CAPG-1 antibodies identify a product of ~160kDa, absent in animals mutant for *capg-1* (Csankovszki et al., 2009)

Strains

All strains were maintained at 20˚C under standard conditions (Brenner, 1974). The following strains were used in this study: wild-type (N2 Bristol), TY4381 {*dpy-28(s939) / qC1 dpy-19(e1259) glp-1(q339)[qIs26] III*}, TY3836 {*dpy-28(y283) / qC1 dpy-19(e1259) glp-1(q339)[qIs26] III*}, TY1550 {*dpy-27(y167) / qC1 dpy-19(e1259) glp-1(q339)[qIs26] III*}, TY3938 {*dpy-26(n199) IV / nT1[let qIs50] IV;V*}, TY4342 {*spo-11(me44) IV / nT1[let qIs50] IV;V*}, TY4394 {*dpy-28(s939) / qC1 dpy-19(e1259) glp-1(q339)[qIs26] III; spo-11(me44) IV / nT1[let qIs50] IV;V*}, VC0531 {*rad-54 and tag-157(ok615) I / hT2[bli-4(e937) let(q782) qIs48] I;III*}, TY5117 {*mix-1(mn29) / mnC1[dpy-10(e128) unc-54(e444)] II*}, TY4546 {*capg-1(tm1514) I / hT2[qIs48] I;IV*}, and TY5118 {*smc-4(tm1860) / qC1 dpy-19(e1259) glp-1(q339)[qIs26] III*}.

All homozygous animals were derived from heterozygous balanced stocks by selecting animals that lacked the dominant balancer-linked marker (Rol or GFP). All heterozygotes were obtained by crossing either N2 Bristol or CB4856 animals into the balanced stock and selecting

animals missing a dominant balancer-linked marker. In cases where a visual marker was not present, the animals were genotyped by PCR.

TUNEL Assay

To detect directly the sites of DNA DSBs, we used terminal dioxynucleotidyl transferase to attach fluorescently labeled nucleotides to exposed 3` DNA ends. Whole mount *C. elegans* gonad samples were prepared as in Tsai et al. (2008). Following 3 10-min washes in PBSt (phosphate buffered saline with 0.1% tween-20), samples were incubated for 30 min in 20 µl of Label Solution from the *In Situ* Cell Death Detection Kit (Fluorescence) (Roche). Most of the Label Solution was wicked away with a Kimwipe and replaced with 20 µl of reaction mixture (2 µl Enzyme Solution and 18 µl Label Solution). Samples were covered with an 18 x 18 mm cover slip and sealed with nail polish. Sealed slides were incubated in a temperature-controlled, variable-power microwave (Microwave Research and Applications, model BP-111-RS) at 37ºC and 75% power for 1 hr. Cover slips were removed with a single edge razor blade and the slides were washed 3 times in PBSt at 37ºC and 75% microwave power for 30 min each. Following a final overnight wash in PBSt at 4ºC, slides were incubated overnight in affinity purified goat anti-fluorescein antibodies (Rockland) diluted 1:250 in PBSt. After 3 10-min washes in PBSt the slides were then incubated in fluorescene-conjugated donkey-anti-goat antibodies (Roche) diluted 1:250 in PBS for 2 hr at 25ºC. Samples were washed 3 times in PBSt for 10 min each and mounted in ProLong Gold (Invitrogen) mounting media containing 1 µg/ml 4',6-diamidino-2-phenylindole (DAPI), covered with a 18 x 18 mm cover slip, cured overnight in the dark, and sealed with nail polish.

TUNEL and RAD-51 Co-staining

TUNEL and RAD-51 co-staining experiments were preformed as for TUNEL alone with the following changes. After microwave incubation with the TUNEL reaction mixture and removal of slide cover slips, the slides were washed only twice for 30 min each in PBSt at 37ºC and 75% microwave power. Following the normal overnight wash in PBSt at 4ºC, the slides were incubated overnight with both affinity purified goat anti-fluorescein antibodies (Rockland) diluted 1:250 in PBSt and rabbit anti-RAD-51 antibodies diluted 1:250 in PBSt. After 3 10-min washes in PBSt the slides were incubated for 2 hr at 25ºC in fluorescene-conjugated donkey-anti-goat antibodies diluted 1:250 in PBSt and Cy3-conjugated donkey-anti-rabbit antibodies (Roche) diluted 1:250 in PBSt. Slides were washed 3 times in PBSt for 10 min each and mounted as in the TUNEL protocol.

Chromosome Axis Length and RAD-51 Distribution Assays

For both chromosomal axis length and RAD-51 distribution assays, whole mount *C. elegans* gonad samples were prepared as in Tsai *et al.* (2008). For X-chromosome studies, FISH was preformed as in (Phillips et al., 2005). The X chromosome right-end probe sequence is 5'-GACTCCATCCACCAGCACTGCTTCGAGTACGACAGAAAGCACTTC-3', and the X chromosome center probe sequence is 5'-TTTCGCTTAGAGCGATTCCTTACCCTTAAATGGGCGCCGG-3'. Chromosome I FISH was preformed as in (Chan et al., 2004), using probes from fosmids (Geneservice) listed in Supplemental Table 3. Following FISH, whole mount slides were incubated with primary antibodies. Guinea pig anti-HTP-3 antibodies and rabbit anti-RAD-51 antibodies were diluted 1:250 in PBS and incubated on the samples overnight at 25˚C. After 3 10-min washes in PBS, Alexa 405 anti-rabbit antibodies and Alexa 633 anti-guinea pig antibodies (Molecular Probes) were diluted 1:250 and simultaneously incubated on slides for 2 hr. After 3 10-min washes in PBS, ProLong Gold mounting media containing 1 µg/ml (DAPI) was added to each slide and covered with an 18 x 18 mm cover slip. Samples were cured overnight in the dark and sealed with nail polish. Nuclei were imaged on a Leica

TCS SP2 AOBS confocal microscope and a 63X 1.4 NA HCX PL APO lens with a voxel size of 40 nm in X, 40 nm in Y, and 80 nm in Z. These datasets were then deconvolved with theoretical point spread function using Huygens Pro or Huygens Essential (Scientific Volume Imaging) deconvolution package. Chromosomes were traced in three dimensions along the HTP-3 staining and straightened using Priism (Chen et al., 1996). Once chromosomes were straightened, the positions of FISH probes, lengths of axis, and RAD-51 foci were measured. For the RAD-51 study, the chromosome was divided into three intervals, delineated by FISH probes, and the percent RAD-51 foci per interval were calculated.

SUPPLEMENTAL REFERENCES

Alpi, A., Pasierbek, P., Gartner, A., and Loidl, J. (2003). Genetic and cytological characterization of the recombination protein RAD-51 in *Caenorhabditis elegans*. Chromosoma *112*, 6-16.

Bhalla, N., and Dernburg, A.F. (2005). A conserved checkpoint monitors meiotic chromosome synapsis in *Caenorhabditis elegans*. Science *310,* 1683-1686.

Brenner, S. (1974). The genetics of *Caenorhabditis elegans*. Genetics *77*, 71-94.

Chan, R.C., Chan, A., Jeon, M., Wu, T.F., Pasqualone, D., Rougvie, A.E., and Meyer, B.J. (2003). Chromosome cohesion is regulated by a clock gene paralogue TIM-1. Nature *423*, 1002-1009.

Chan, R.C., Severson, A.F., and Meyer, B.J. (2004). Condensin restructures chromosomes in preparation for meiotic divisions. J. Cell Biol. *167*, 613-625.

Chuang, P.T., Albertson, D.G., and Meyer, B.J. (1994). DPY-27:a chromosome condensation protein homolog that regulates *C. elegans* dosage compensation through association with the X chromosome. Cell *79*, 459-474.

Couteau, F., Nabeshima, K., Villeneuve, A., and Zetka, M. (2004). A component of C. elegans meiotic chromosome axes at the interface of homolog alignment, synapsis, nuclear reorganization, and recombination. Curr. Biol. *14*, 585-592.

Csankovszki, G., Collette, K., Spahl, K., Carey, J., Snyder, M., Petty, E., Patel, U., Tabuchi, T., Liu, H., McLeod, I.*, et al.* (2009). Three distinct condensin complexes control *C. elegans* chromosome dynamics. Curr. Biol. *19*, 9-19.

Hagstrom, K.A., Holmes, V.F., Cozzarelli, N.R., and Meyer, B.J. (2002). *C. elegans* condensin promotes mitotic chromosome architecture, centromere organization, and sister chromatid segregation during mitosis and meiosis. Genes Dev. *16*, 729-742.

Holzen, T.M., Shah, P.P., Olivares, H.A., and Bishop, D.K. (2006). Tid1/Rdh54 promotes dissociation of Dmc1 from nonrecombinogenic sites on meiotic chromatin. Genes Dev. *20*, 2593-2604.

Lieb, J.D., Capowski, E.E., Meneely, P., and Meyer, B.J. (1996). DPY-26, a link between dosage compensation and meiotic chromosome segregation in the nematode. Science *274*, 1732-1736.

Phillips, C.M., Wong, C., Bhalla, N., Carlton, P.M., Weiser, P., Meneely, P.M., and Dernburg, A.F. (2005). HIM-8 binds to the X chromosome pairing center and mediates chromosome-specific meiotic synapsis. Cell *123*, 1051-1063.

Tsai, C.J., Mets, D.G., Albrecht, M.R., Nix, P., Chan, A., and Meyer, B.J. (2008). Meiotic crossover number and distribution are regulated by a dosage compensation protein that resembles a condensin subunit. Genes Dev. *22*, 194-211.

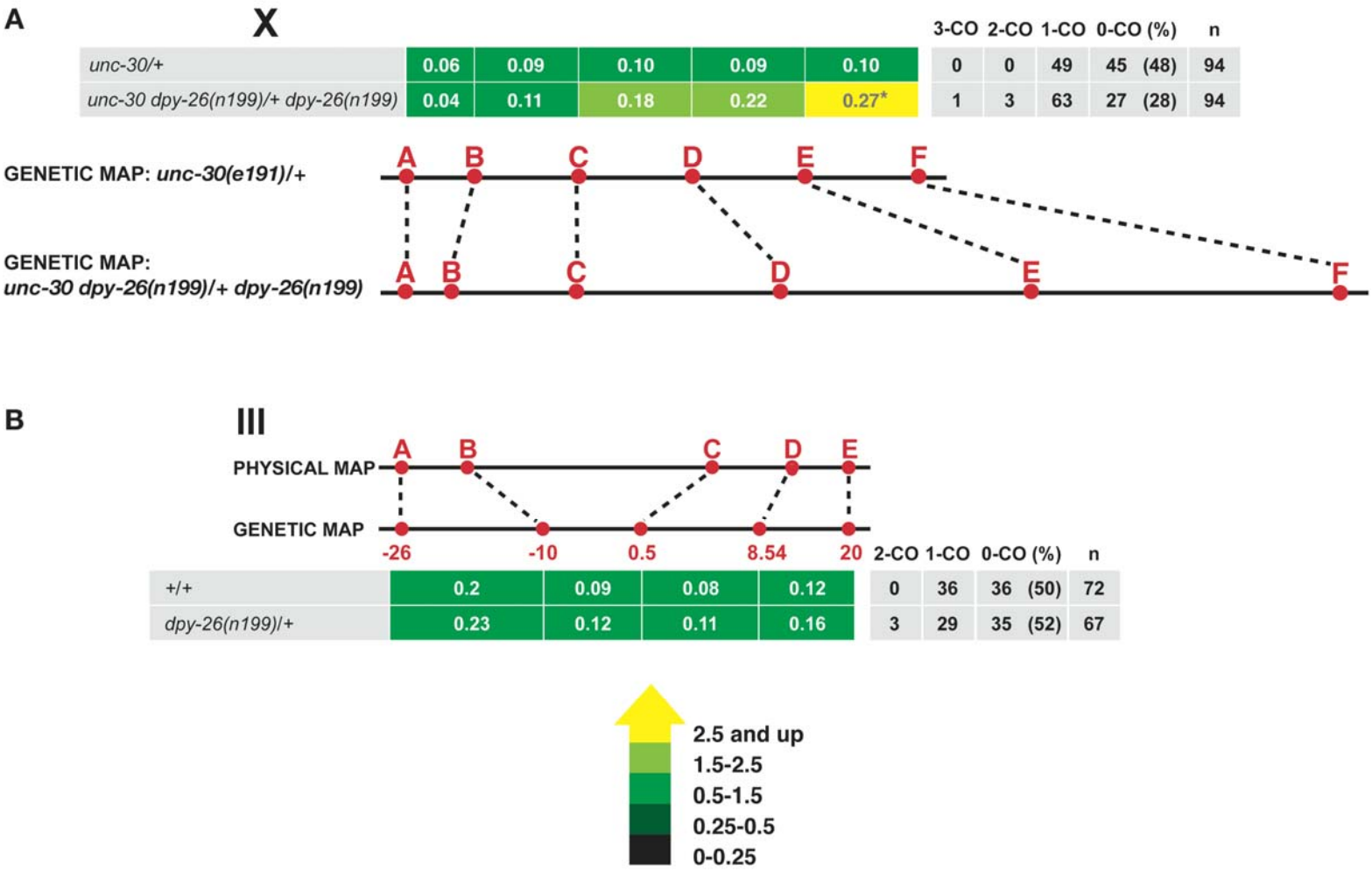

Figure S1. *dpy-26* Mutations Increase CO Frequency and Shift CO Distribution on Chromosomes X and III

(A-B) Crossover analysis of chromosomes X and III in wild-type and *dpy-26(n199)* animals. For each genotype (left), the CO frequencies are shown in white numbers in the colored boxes. CO frequencies were calculated by the formula (number of COs in the interval)/(total meiotic products assayed). The box colors represent the relative recombination frequencies in each interval between mutant and wild-type animals; the key is at the bottom. Shown to the right are the number of triple (3-CO), double (2-CO), single (1-CO), and non (0-CO) crossover chromatids as well as the total number (n) of chromatids scored. (%) Percentage of 0-COs was calculated by the formula 100(0-CO/n). (A) Comparison of X-chromosome genetic maps in wild-type and homozygous *dpy-26* mutant hermaphrodites, showing the genetic positions of SNP markers (red) used to map CO sites are shown below the color-coded map. The length of line between SNP markers is proportional to the CO frequency in that interval and is a spatial representation of changes in CO frequency. Asterisk identifes a CO interval statistially different ($p < 0.01$) from that in wild-type animals, as shown by the Fisher's exact test. (B) The relative physical and genetic positions of SNP markers (red) on chromosome III used to map CO sites are shown above the chart. An increase in 2-CO number was evident on chromosome III of *dpy-26* null mutants compared to wild-type animals ($p < 0.1$).

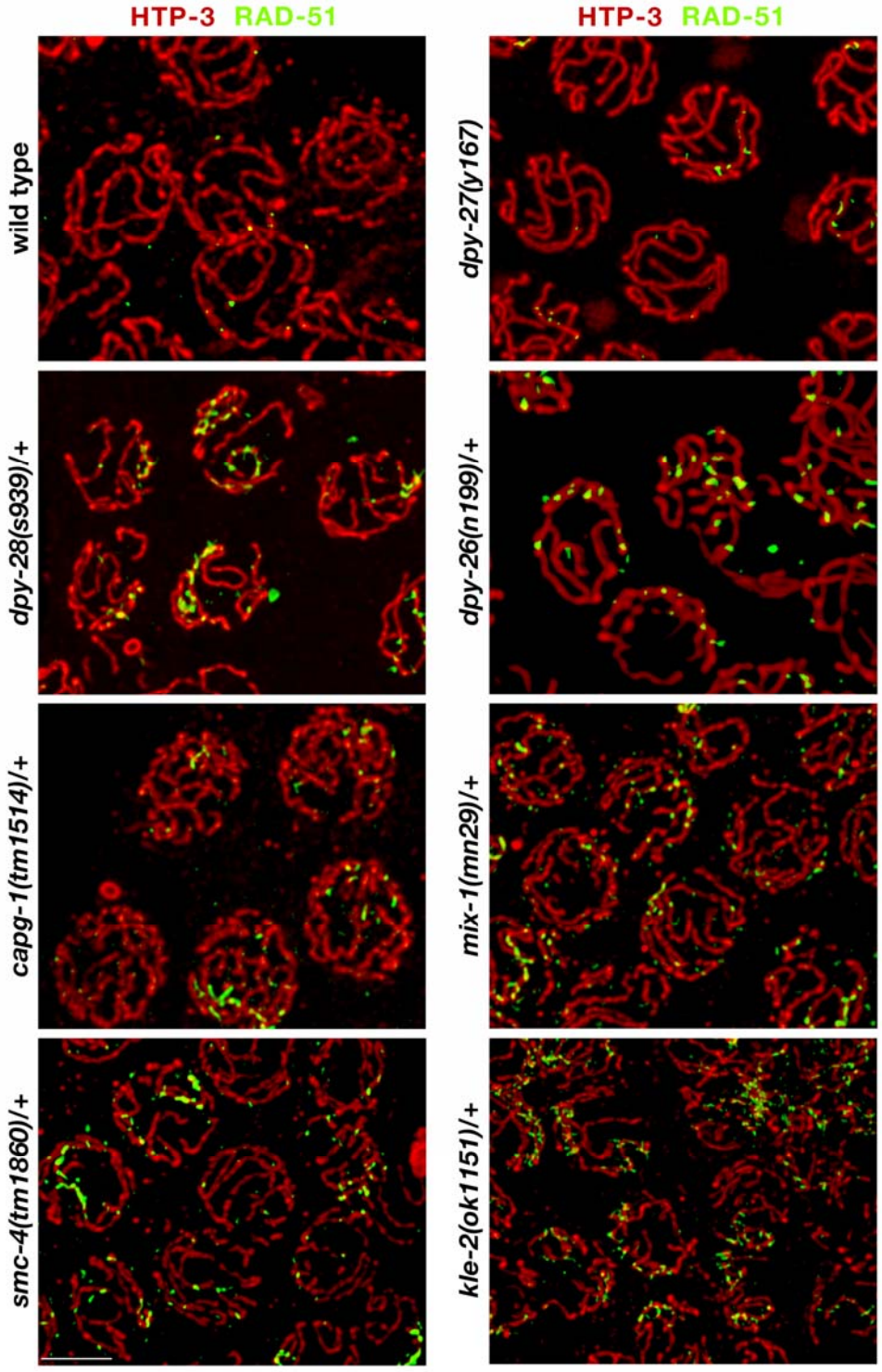

Figure S2. Mutations in Each Gene Encoding a Condensin I Subunit Cause an Increase in RAD-51 Foci

Shown are high resolution confocal images of pachytene nuclei labeled with antibodies against the chromosomal axis protein HTP-3 (red) and the DSB repair protein RAD-51 (green). Heterozygous null mutations in any gene encoding a condensin I subunit cause an increase in RAD-51 foci, while complete disruption of the condensin I^{DC}-specific gene *dpy-27* does not. Animals heterozygous for a null mutation in the gene encoding condensin II subunit KLE-2 also exhibit an increase in RAD-51 foci. For all images, genotypes of the nuclei depicted are shown at the left. Scale bar, 4 μm.

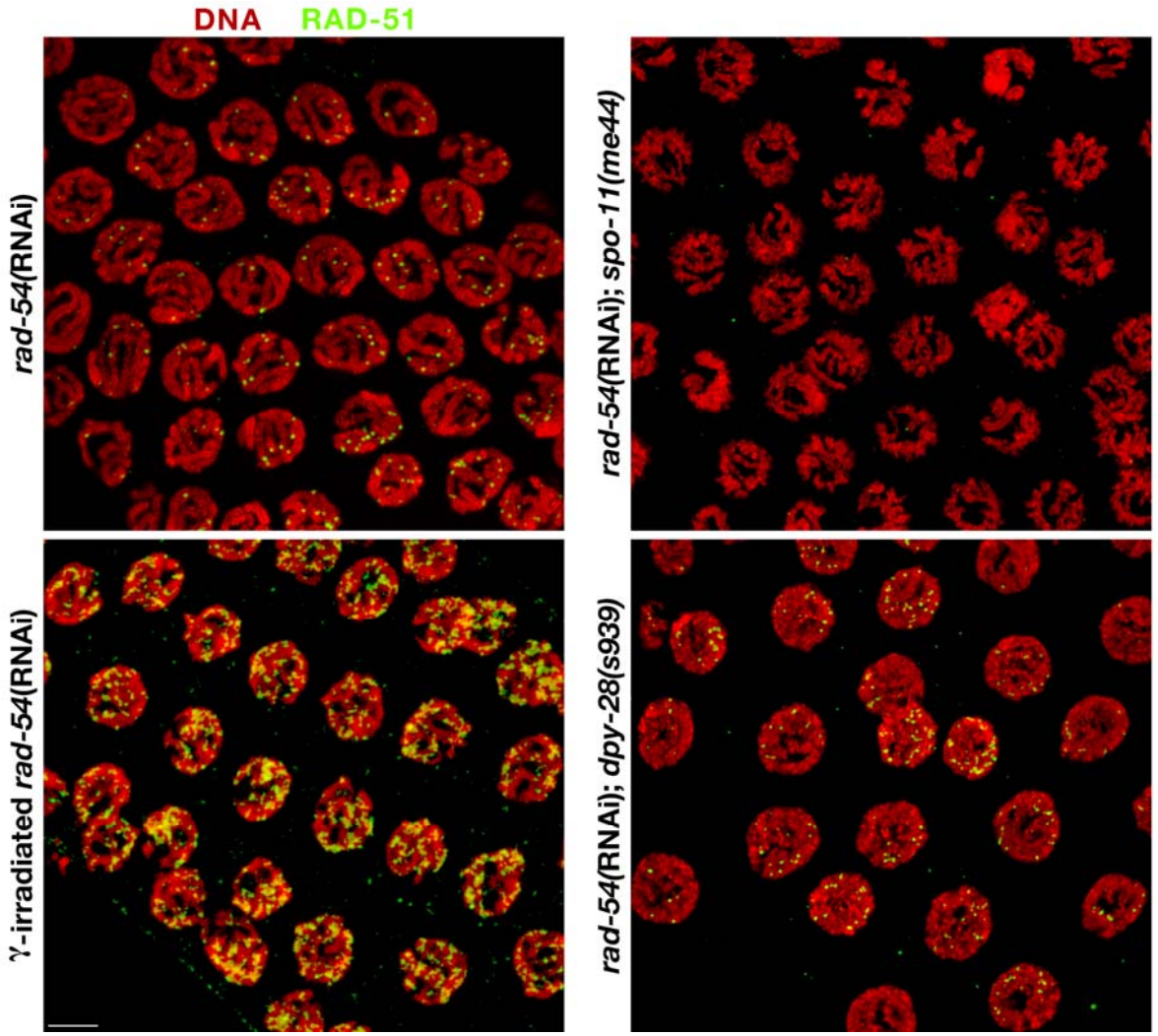

Figure S3. Effect of *rad-54*(RNAi) on RAD-51 Foci
Shown are high resolution confocal images of pachytene nuclei labeled with DAPI (red) and RAD-51 antibodies (green). For all images, the genotype of the animal depicted is shown at the left. γ-irradiation of *rad-54*(RNAi) animals induces more RAD-51 foci, indicating that RAD-51 is not limiting in quantity in the *rad-54* RNAi-treated animals. No RAD-51 foci were detected in *rad-54*(RNAi); *spo-11(me44)* mutants, indicating that DSBs are not made independently of SPO-11 in *rad-54*(RNAi) animals. *dpy-28(s939);rad-54*(RNAi) animals have more RAD-51 foci than *rad-54*(RNAi) animals. Scale bar, 4 μm.

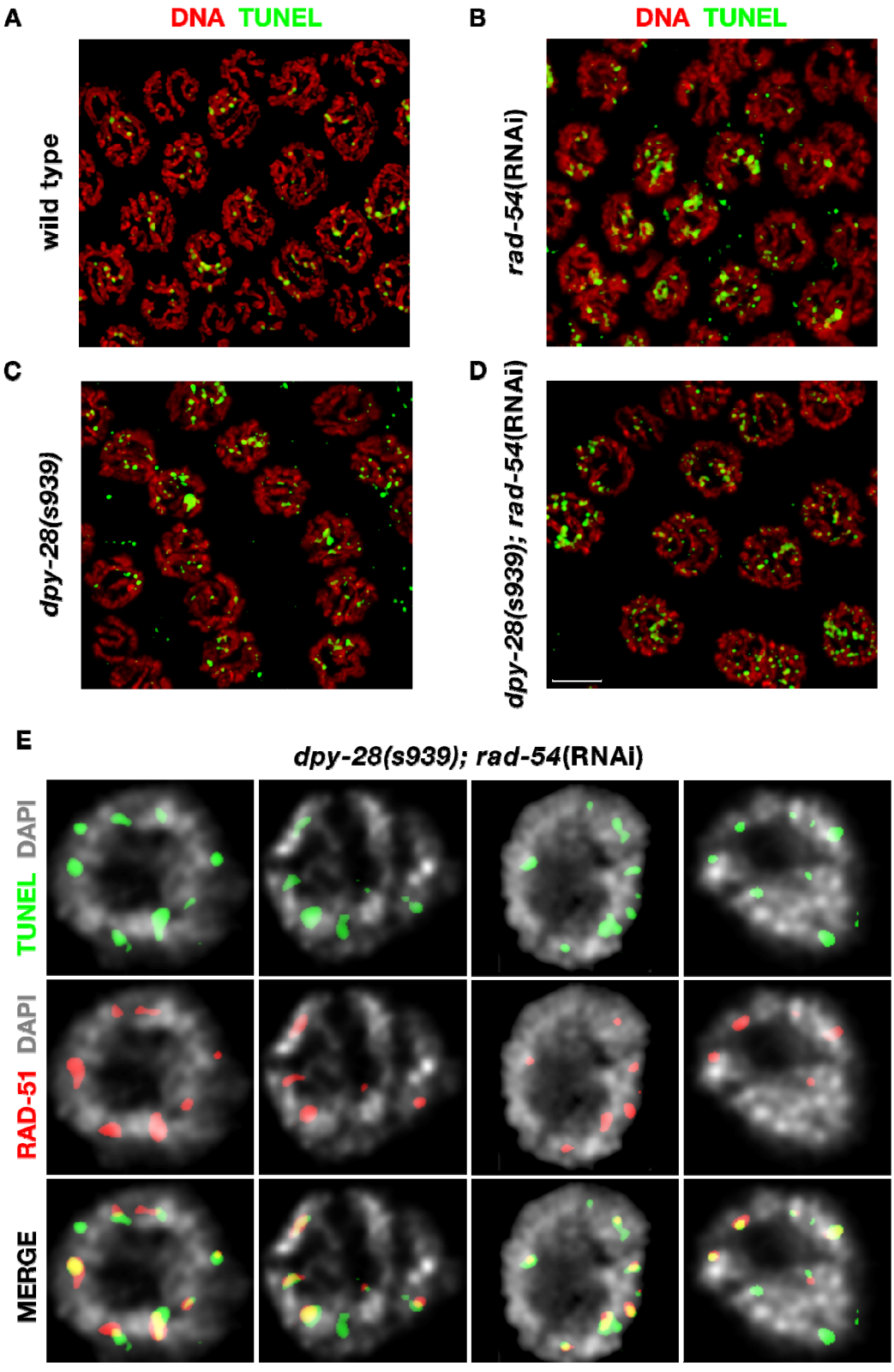

Figure S4. The *dpy-28(s939)* Mutation Increases the Number of Meiotic Double Strand Breaks
(A-D) Shown are high resolution confocal images of pachytene nuclei from wild-type, *dpy-28(s939)*, *rad-54*(RNAi), and *dpy-28(s939); rad-54*(RNAi) animals labeled with DAPI (red) and TUNEL reagents (green). *dpy-28(s939)* animals have more TUNEL foci than wild-type animals, consistent

with an increase in DSBs in *dpy-28(s939)*. However, slowing the rate of DSB repair could explain the increase in TUNEL foci. Because *rad-54*(RNAi) prevents repair of DSBs by homologous recombination (Figures 4 and 5), the number of TUNEL foci present in *rad-54*(RNAi) conditions should indicate the total number of DSBs formed, independent of DSB repair kinetics. *dpy-28(s939);rad-54*(RNAi) mutants have more TUNEL foci than *rad-54*(RNAi) animals. Thus, the *dpy-28(s939)* mutation increases the number of meiotic DSBs. For all images, the genotype of the animal depicted is shown at the left. Scale bar, 4 μm.

(E) Shown are high resolution partial projections of pachytene nuclei from *dpy-28(s939); rad-54*(RNAi) animals labeled with DAPI (gray), RAD-51 antibodies (red), and TUNEL reagents (green). Consistent with the quantification (Figure S5), all foci positive for RAD-51 are also positive for TUNEL staining, while some foci are only positive for TUNEL signal. The conditions optimal for TUNEL staining are not optimal for RAD-51 staining, as show by comparison of Figures 4D, 4E, S5A-S5E, S5I, S5J, and S5K. Nevertheless, the distribution of TUNEL and RAD-51 foci is the same in singly labeled germlines (Figures 4D and E). Scale bar, 1 μm.

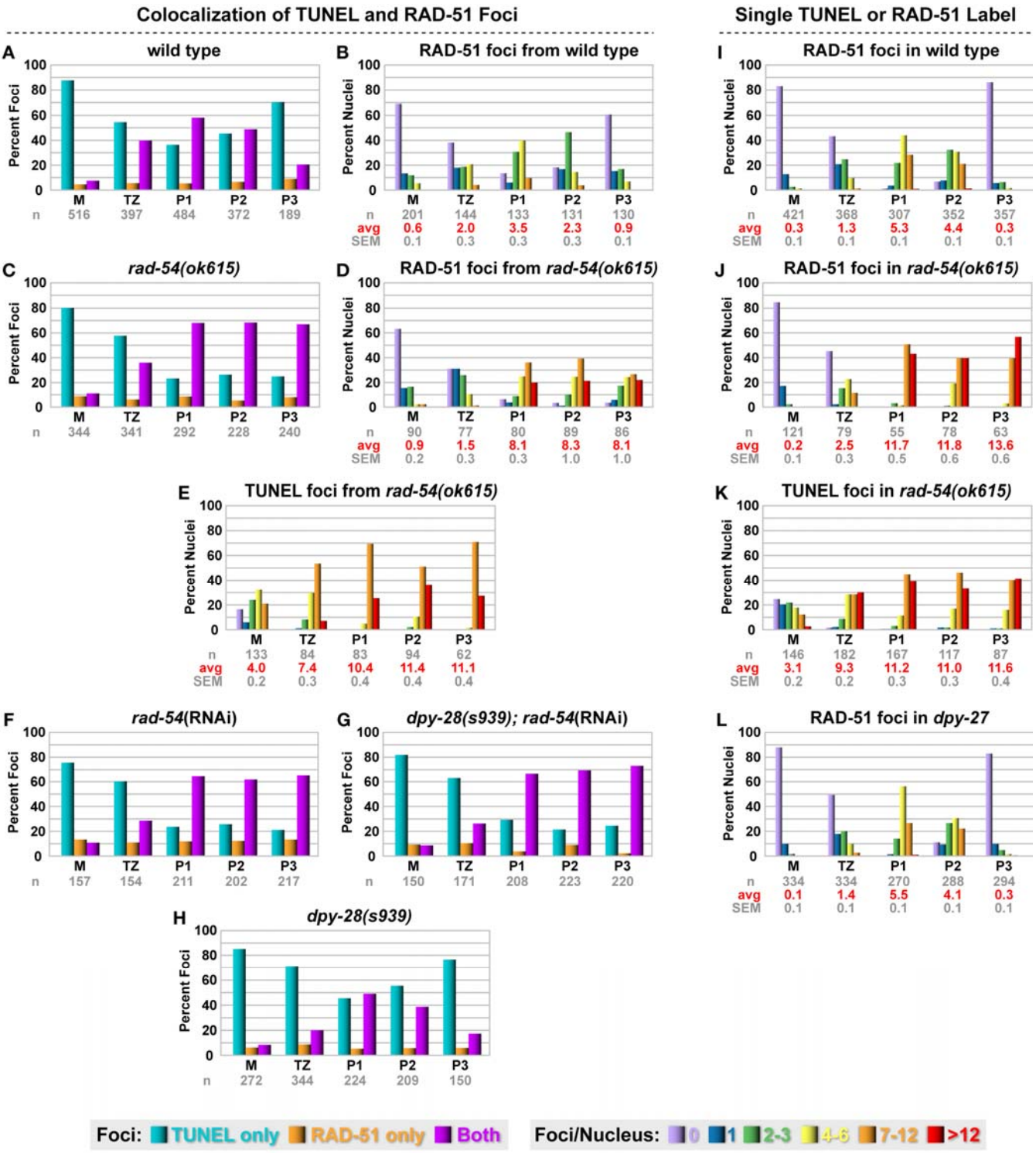

Figure S5. Co-localization of TUNEL and RAD-51 Foci and analysis of RAD-51 in *dpy-27* Null Mutants

(A, C, F-H) Histograms show quantification of foci positive for both RAD-51 and TUNEL signals (purple), TUNEL only (blue), and RAD-51 only (orange) in germlines of indicated genotypes stained for both. The Y-axis shows the percentage of foci in each class. The X-axis shows the position along the germline: pre-meiotic region (M), transition zone (TZ), the first third of pachytene (P1), the second third of pachytene (P2), and the last third of pachytene (P3). (n) is the total number of foci in each stage.

(B) Histogram shows quantification of RAD-51 foci in wild-type germlines of panel A co-stained for TUNEL and RAD-51.

(D,E) Histograms shows quantification of RAD-51 or TUNEL foci in *rad-54(ok615)* germlines of panel C co-stained for TUNEL and RAD-51.

(I-L) Histograms show quantification of RAD-51 or TUNEL foci in germlines stained for RAD-51 or TUNEL only.

(B, D, E, I-L) X-axis is as above, except that (n) is the number of nuclei scored, (avg) is the average number of foci, and (SEM) is the standard error of the mean for each stage. Y-axis is the percent of nuclei in each class; the key is below the histograms.

(A-E, I-K) In gonads from both wild-type and *rad-54(ok615)* animals, a significant fraction of foci in TZ, P1 and P2 stages are positive for both TUNEL and RAD-51, suggesting that RAD-51 is a good marker for DSBs. As expected, most foci in the pre-meiotic region of germlines from both wild-type and *rad-54(ok615)* animals are only positive for TUNEL signal, likely resulting from nicks associated with replication. In P3 of wild-type germlines, fewer foci are positive for both TUNEL and RAD-51 than TUNEL alone, possibly the result of RAD-51 removal before ligation of nicked DNA. Consistent with this conclusion, most foci in P3 of gonads from *rad-54(ok615)* animals, in which RAD-51 removal is impaired, are positive for both TUNEL and RAD-51 signals. In budding yeast, mutations in *rad54*, the homolog of *C. elegans rad-54*, can cause an increase in RAD51 foci not associated with DSBs (Holzen et al., 2006). Were the same phenomenon to occur in *C. elegans,* it must occur at a low level, because in *rad-54* mutants, there are always fewer foci that are only positive for RAD-51 signal than foci only positive for TUNEL signal or foci positive for both RAD-51 and TUNEL signal. Surprisingly, P1 and P2 of germlines from both wild-type animals and *rad-54(ok615)* have a significant fraction of foci that are only positive for TUNEL signal. This was an unexpected result as there are similar numbers of TUNEL or RAD-51 foci in gonads independently labeled for either TUNEL or RAD-51 (Figure 4D-G, J, K). The lower level of RAD-51 foci in co-stained germlines compared to RAD-51 singly stained germlines is due to the loss of the RAD-51 epitope, likely because of the harsh conditions used to facilitate TUNEL, as shown in the comparison of (B, D) to (I, J). Importantly, co-staining for RAD-51 and TUNEL foci did not cause more TUNEL foci than in germlines stained for TUNEL only, as shown by comparison of (E) and (K).

(F-H) The *dpy-28(s939)* mutation does not change the relative percentages of foci positive for TUNEL only, RAD-51 only, or TUNEL and RAD-51 compared to those in wild-type animals. *dpy-28(s939)* mutations could change the number of DSBs that are repaired through a RAD-51 intermediate and thereby increase sites available for a CO. If that were true, the relative percentage of foci in each of the three categories (TUNEL only, RAD-51 only, and TUNEL and RAD-51) would change in the *dpy-28(s939)* background. However, it did not. Furthermore, the relative percentage of foci in each category is the same in *rad-54*(RNAi) and *dpy-28(s939); rad-54*(RNAi) germlines, for which DSB repair via RAD-51 is inhibited.

(I, L) The number of RAD-51 foci in mutants homozygous for a null mutation in the dosage compensation-specific gene *dpy-27 i*s not higher than in wild-type germlines.

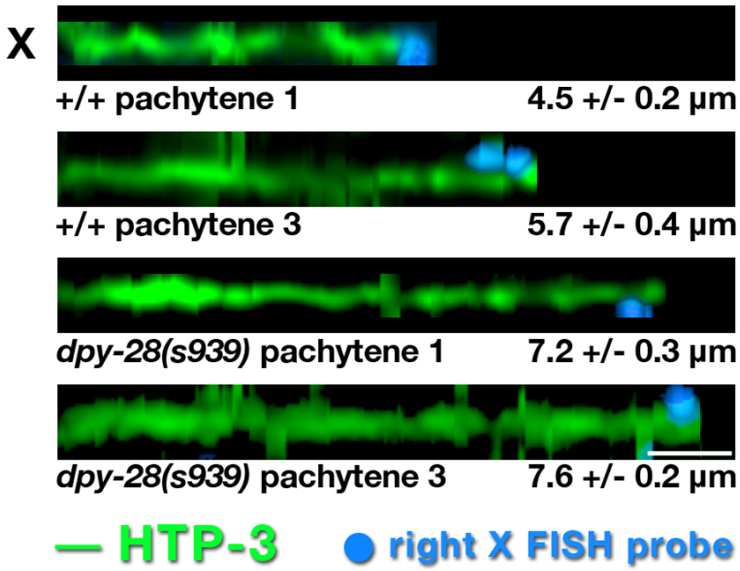

Figure S6. The X Axis of *dpy-28(s939)* Mutants Is Expanded Throughout Pachytene
Shown are straightened and horizontally displayed X axes from wild-type and *dpy-28(s939)* animals. Nuclei from the first third and last third of pachytene were labeled with the axis component HTP-3 (green) and the X-chromosome FISH probe at the right end (blue). Genotypes, pachytene stage, average total axis length, and standard error of the mean are shown below each axis. Scale bar, 1 µm.

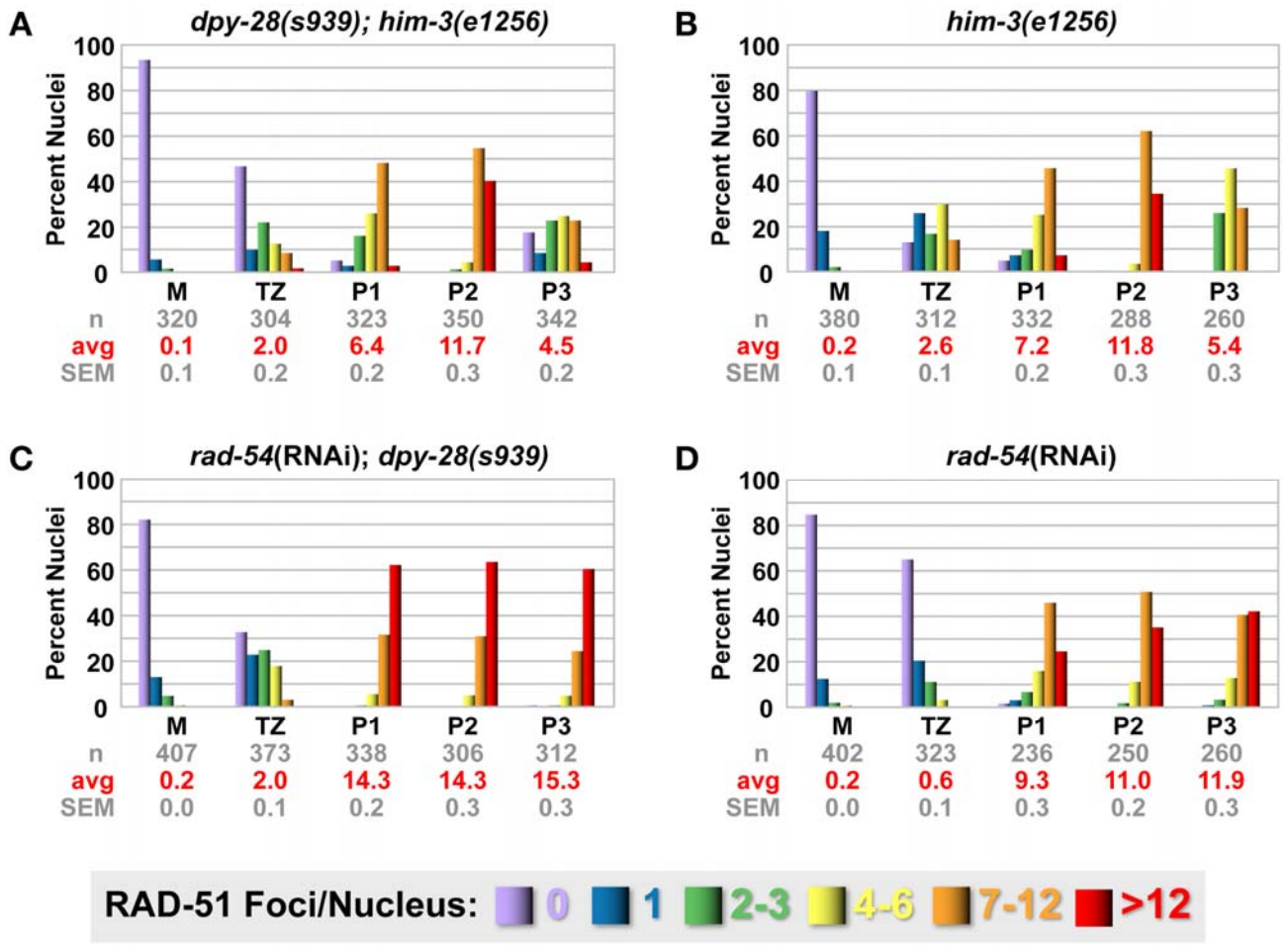

Figure S7. The DSB Increase in Condensin I Mutants Requires the Axis Protein HIM-3
(A-D) Histograms show quantification of RAD-51 foci in germlines of *dpy-28(s939); him-3(e1256)*, *him-3(e1256)*, *rad-54*(RNAi); *dpy-28(s939)*, or *rad-54*(RNAi) animals. Each column color represents a class of nuclei with the indicated number of foci. The Y-axis shows the percentage of foci in each class. The X-axis shows the position along the germline: pre-meiotic (M), transition zone (TZ), the first third of pachytene (P1), the second third of pachytene (P2), and the last third of pachytene (P3). The number of nuclei (n), average number of foci (avg), and standard error of the mean (SEM), are shown beneath each stage.

The axis-associated protein HIM-3 is required for homolog pairing and synapsis, and it biases meiotic CO recombination between homologs rather than sisters (Couteau et al., 2004). In *him-3* null mutants, homologs cannot pair or synapse; however, normal levels of RAD-51 foci appear and disappear with wild-type kinetics, suggesting that DSB initiation is normal, but DSB repair is carried out using sister chromatids as templates (Couteau et al., 2004). The *him-3* null mutation suppresses the increase in RAD-51 foci caused by *dpy-28* mutations (Tsai et al., 2008). Here we show a similar result with the *him-3(e1256)* missense, partial-loss-of-function mutation T24M. This mutation, unlike the null mutation, causes a peak accumulation of RAD-51 foci comparable to that in *rad-54*(RNAi) animals (~12), which have severely compromised DSB repair. However, unlike *rad-54*(RNAi) animals, *him-3(e1256)* mutants repair DSBs, albeit incompletely, at the end of pachytene (~ 5 RAD-51 foci). The levels of RAD-51 foci are equivalent in *dpy-28(s939); him-3(e1256)* and *him-3(e1256)* mutants, but lower than in *rad-54*(RNAi); *dpy-28(s939)* mutants, indicating that the *him-3(e1256)* mutation suppresses the increase in DSBs caused by *dpy-28* mutations. Thus, the effect of *dpy-28*

mutations on DSBs is dependent on an intact axis. Figure 7 of the main text shows that the *him-3(e1256)* mutation also suppresses the axis expansion caused by *dpy-28* mutations, consistent with the view that chromosome structure imposed by condensin I likely plays a significant role in DSB distribution.

Figure S8.

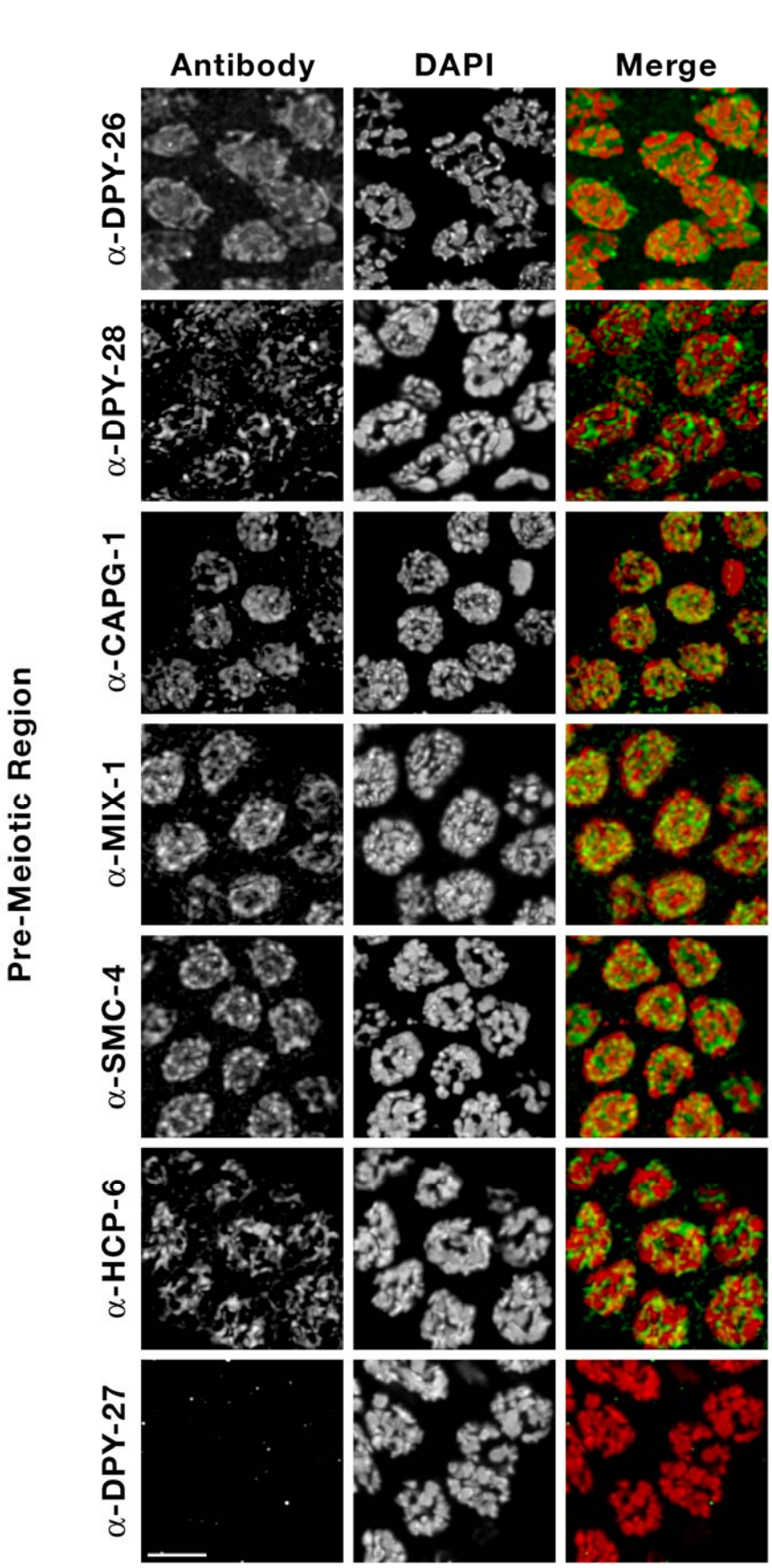
A
Antibody
DAPI
Merge
Pre-Meiotic Region
α-DPY-26
α-DPY-28
α-CAPG-1
α-MIX-1
α-SMC-4
α-HCP-6
α-DPY-27

B

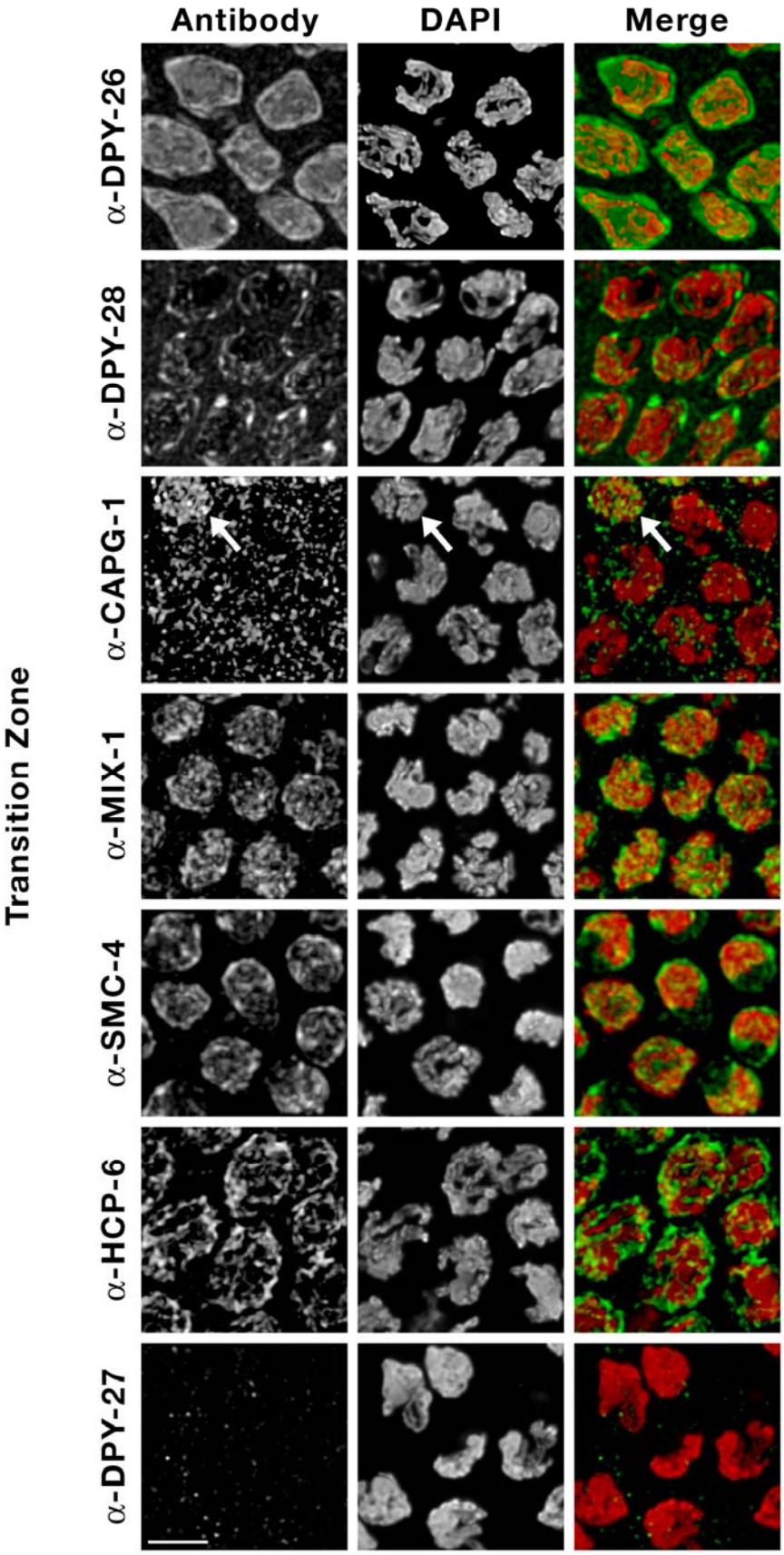
Antibody
DAPI
Merge
α-DPY-26
α-DPY-28
α-CAPG-1
α-MIX-1
α-SMC-4
α-HCP-6
α-DPY-27
Transition Zone

C

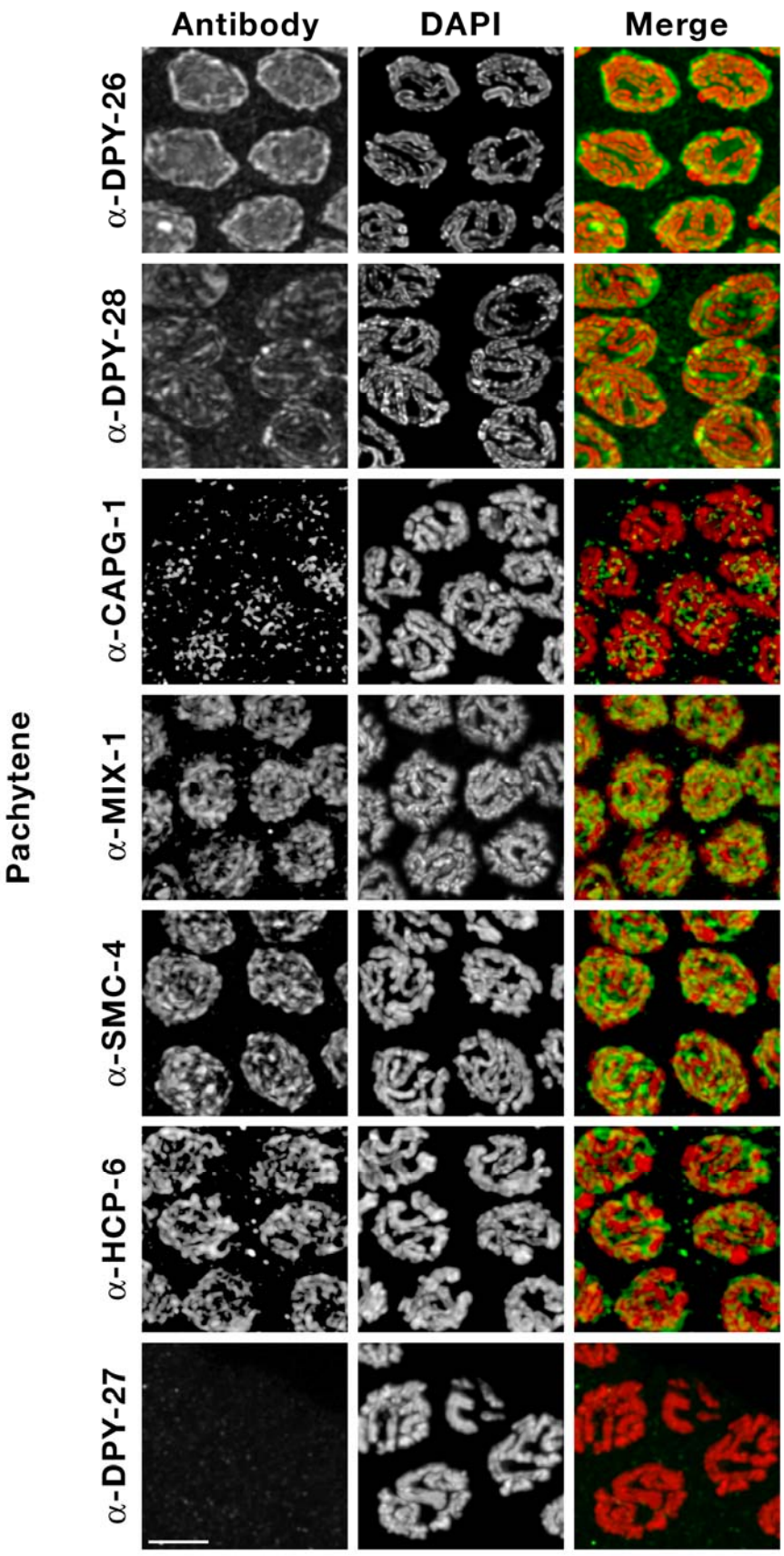
Antibody
DAPI
Merge
Pachytene
α-DPY-26
α-DPY-28
α-CAPG-1
α-MIX-1
α-SMC-4
α-HCP-6
α-DPY-27

Figure S8. All Subunits of Condensin I and Condensin II are Enriched in Germline Nuclei, but Condensin I^{DC}-specific Subunit DPY-27 Is Not.

Shown are high resolution confocal images of germline nuclei from the pre-meiotic (A), transition zone (B), and pachytene (C) stages of the germline. Nuclei are labeled with DAPI (red) and antibodies (green) to either DPY-28, DPY-26, or CAPG-1 subunits of both condensin I and condensin I^{DC} complexes, SMC-4, a subunit of both condensin I and condensin II, MIX-1, a subunit of condensin I, condensin II, and condensin I^{DC} HCP-6, a protein specific to condensin II, or DPY-27, a condensin I^{DC} subunit. Our previous work demonstrated that condensin II subunit HCP-6 is highly enriched on DNA at pachytene exit (Chan et al., 2004). Here we show that, in every prior germline stage, all condensin I or condensin II subunits are enriched in nuclei, and partially overlap with DNA. In contrast, the condensin I^{DC}-specific protein DPY-27 is absent in all three stages of the germline. For all images, the antibody used is shown at the left. The arrow (B) points to a pre-meiotic nucleus, which highlights the finding that CAPG-1 is more abundant in pre-meiotic germ cells than in meiotic cells. The lower abundance explains why the SMC-4 IP recovered less CAPG-1 than any other condensin I subunit. Scale bar, 4 μm.

Table S1. Peptides Identified by MALDI-TOF Mass Spectrometry of Trypsanized Proteins Immuno-precipitated with DPY-26 Antibodies

SMC-4			MIX-1			DPY-27			DPY-28			DPY-26		
Peptide Masses	**Difference**	**Residues**	**Peptide Masses**	**Difference**	**Residues**	**Peptide Masses**	**Difference**	**Residues**	**Peptide Masses**	**Difference**	**Residues**	**Peptide Masses**	**Difference**	**Residues**
884.4466	**-0.0012**	**957-963**	**893.4869**	**0.0024**	**227-233**	**914.5466**	**0.0043**	**872-879**	**890.5748**	**0.0033**	**1293-1300**	**884.4972**	**0.0196**	**298-304**
897.5165	**0.0007**	**1361-1368**	**895.4473**	**0.0199**	**79-85**	**914.5466**	**0.0043**	**873-880**	**917.4807**	**-0.0038**	**1099-1107**	**920.5785**	**-0.0036**	**221-228**
902.5073	**0.0013**	**587-593**	**910.5642**	**-0.0084**	**869-877**	**926.4634**	**0.0037**	**399-405**	**941.4728**	**-0.0005**	**1211-1218**	**963.4876**	**-0.0024**	**207-214**
915.4692	**-0.0030**	**302-309**	**915.5507**	**-0.0008**	**808-815**	**932.4927**	**-0.0027**	**392-398**	**948.4930**	**0.0027**	**519-525**	**1001.5390**	**-0.0030**	**525-533**
922.5055	**-0.0017**	**310-317**	**916.4859**	**-0.0033**	**5-12**	**948.5311**	**-0.0108**	**108-115**	**978.5024**	**0.0015**	**300-308**	**1002.5068**	**0.0059**	**256-263**
924.4705	**0.0053**	**1207-1213**	**1062.5579**	**-0.0005**	**199-207**	**1169.6262**	**0.0082**	**797-806**	**992.5337**	**0.0019**	**929-936**	**1060.5663**	**0.0024**	**369-378**
954.4631	**0.0098**	**186-193**	**1065.5688**	**-0.0005**	**498-506**	**1174.6969**	**0.0021**	**1299-1308**	**1040.5452**	**0.0035**	**509-516**	**1101.5468**	**-0.0112**	**1068-1076**
1003.5295	**0.0082**	**487-494**	**1105.5908**	**0.0015**	**268-276**	**1533.7498**	**-0.0051**	**433-445**	**1041.5834**	**-0.0223**	**638-646**	**1188.6608**	**0.0020**	**368-378**
1026.5804	**-0.0031**	**625-634**	**1125.6128**	**-0.0001**	**700-708**	**1569.8647**	**-0.0034**	**129-142**	**1076.5518**	**0.0029**	**488-497**	**1194.6450**	**-0.0033**	**54-64**
1039.5905	**0.0005**	**1197-1205**	**1132.5643**	**0.0004**	**851-859**	**1585.8615**	**-0.0127**	**611-624**	**1092.5432**	**0.0073**	**647-655**	**1306.6294**	**0.0015**	**871-881**
1052.5624	**0.0023**	**1206-1213**	**1132.5643**	**0.0004**	**850-858**	**1599.7634**	**0.0123**	**184-196**	**1140.6127**	**0.0074**	**86-95**	**1322.7321**	**-0.0111**	**54-65**
1106.5791	**-0.0055**	**1274-1283**	**1198.5804**	**-0.0012**	**1095-1105**				**1141.5836**	**0.0194**	**875-883**	**1350.7346**	**0.0003**	**341-351**
1108.5294	**0.0084**	**1340-1348**	**1215.5752**	**0.0146**	**350-360**				**1142.5743**	**0.0036**	**1301-1310**	**1363.7063**	**0.0093**	**203-214**
1110.5487	**-0.0057**	**222-230**	**1261.6714**	**-0.0231**	**526-536**				**1153.6742**	**0.0049**	**783-792**	**1365.6516**	**0.0077**	**1198-1207**
1131.6422	**-0.0104**	**660-669**	**1266.6458**	**0.0016**	**375-384**				**1219.6847**	**0.0048**	**498-508**	**1382.6620**	**0.0028**	**534-545**
1157.6541	**0.0011**	**563-572**	**1296.6434**	**0.0064**	**61-72**				**1220.6866**	**0.0002**	**342-351**	**1383.6696**	**-0.0001**	**785-795**
1162.6624	**0.0040**	**1316-1325**	**1346.7128**	**-0.0039**	**986-996**				**1269.5590**	**0.0090**	**97-106**	**1423.6095**	**0.0118**	**16-27**
1167.6873	**0.0023**	**1197-1206**	**1419.6937**	**-0.0071**	**1233-1244**				**1287.6638**	**0.0046**	**628-637**	**1511.7589**	**-0.0058**	**784-795**
1233.6561	**-0.0217**	**1259-1269**	**1435.6724**	**-0.0021**	**967-979**				**1312.6637**	**0.0027**	**1017-1027**	**1525.7793**	**-0.0143**	**77-89**
1266.6564	**0.0009**	**221-230**	**1456.7949**	**-0.0062**	**1199-1212**				**1320.6853**	**0.0053**	**684-695**	**1569.8647**	**-0.0027**	**40-53**
1298.6278	**0.0050**	**532-542**	**1462.7648**	**-0.0006**	**746-758**				**1425.6605**	**0.0094**	**96-106**	**1599.7634**	**0.0019**	**134-147**
1314.6725	**0.0071**	**432-443**	**1590.8085**	**-0.0002**	**931-944**				**1433.6897**	**0.0043**	**546-556**	**1610.8295**	**0.0018**	**484-497**
1368.7551	**0.0024**	**174-185**	**1613.7726**	**-0.0020**	**1162-1175**				**1438.6890**	**0.0022**	**265-275**	**1714.8496**	**-0.0003**	**796-810**
1404.7915	**0.0064**	**1328-1339**							**1453.7412**	**0.0013**	**389-401**	**1772.8141**	**0.0016**	**665-680**
1410.6971	**0.0066**	**1248-1258**										**1796.8049**	**0.0110**	**554-568**
1472.7916	**0.0054**	**687-700**										**1832.8606**	**-0.0074**	**750-765**
1491.8085	**0.0026**	**647-659**												
1510.7190	**0.0012**	**1412-1424**												
1553.7684	**0.0044**	**1219-1231**												

This table lists the masses in daltons of predicted tryptic peptides from SMC-4, MIX-1, DPY-27, DPY-28, and DPY-26, which match the measured masses of tryptic peptides obtained from proteins precipitated with DPY-26 antibodies (Figure 1A). Deviations from the predicted mass are provided (Difference) as well as peptide positions within the full length protein (Residues). Peptide masses were matched against predicted open reading frames using the search program MS-fit.

Table S2. Snip-SNP Markers on Chromosome III Used for Crossover Analysis

snip-SNP	cosmid	map position	primer sequence(5`-3`)	restriction enzyme	N2 restriction fragments (bp)	CB4856 restriction fragments (bp)
IIIA	T17H7	-26	Forward: ctgcttatagtcttcctgtcg Reverse: gcaaccccaccttcaatgac	SspI	910	580, 330
IIIB	H06I4	-10	Forward: aaaccacctgaaactggagc Reverse: ctcgagattctgcgtgaaac	SpeI	438	268, 170
IIIC	F10E9	0.5	Forward: agcagatgaaagttccgacg Reverse: ccccgctgtggttattatac	AccI	598, 255	854
IIID	T28D6	8.5	Forward: tttcgtgtacgaacgtctcc Reverse: catttctcccactcttgctg	DraI	500	283, 217
IIIE	F54F12	20	Forward: ttgactcttctggagtagctgc Reverse: ggattccagggattgaagag	RsaI	385,76, 11	207,178,76,11

Table S3. Fosmids Used to Create Chromosome I FISH Probes

Probe	Chromosome	Fosmid	Start position (bp)	Stop position (bp)
1	I	WRM062bF03	2776181	2810622
1	I	WRM0617bF07	2788401	2820631
1	I	WRM0635aF10	2802243	2836479
1	I	WRM062dG04	2813818	2846292
1	I	WRM0621dG02	2952955	2985165
2	I	WRM067cF06	12562475	12595314
2	I	WRM0624dH02	12566438	12605809
2	I	WRM0612aE11	12592672	12625453
2	I	WRM066cD10	12615203	12649390
2	I	WRM0629bB02	12635816	12671885